Augmentation of post-swelling surgical sealant potential of adhesive hydrogels

Tarek M. Shazly[a,*], **Aaron B. Baker**[a], **John R. Naber**[b], **Adriana Bon**[a], **Krystyn J. Van Vliet**[c], and **Elazer R. Edelman**[a,d]

[a]Harvard–MIT Division of Health Sciences and Technology, Massachusetts Institute of Technology, Cambridge, Massachusetts 02139

[b]Department of Chemistry, Massachusetts Institute of Technology, Cambridge, Massachusetts 02139

[c]Department of Materials Science and Engineering, Massachusetts Institute of Technology, Cambridge, Massachusetts 02139

[d]Cardiovascular Division, Department of Medicine, Brigham and Women's Hospital, Harvard Medical School, Boston, Massachusetts 02115

Abstract

Two-component hydrogels formed with star polyethylene glycol amine and linear dextran aldehyde polymers (PEG:dextran) show promise as tissue-specific surgical sealants. There is however a significant loss of adhesion strength to soft tissues following PEG:dextran swelling, which may limit material ability to appose disjoined tissues and prevent leakage from surgical sites. We covalently incorporated the modified amino acid L-3,4-dihydroxyphenylalanine (L-DOPA) into PEG:dextran to enhance post-swelling sealant performance. L-DOPA is an essential component of marine animal adhesive plaques and has been used to confer wet adhesion in synthetic materials. As both PEG:dextran cohesion and adhesion are mediated by aldehyde-amine interactions, L-DOPA side-groups make it a potent network modulator with potential to affect multiple material properties. Following one hour submersion in aqueous media, PEG:dextran doped with 3 mM L-DOPA/M aldehyde on average swelled 50.3% less, had 287.4% greater stiffness and had 53.6% greater functional adhesion strength compared to the neat hydrogel. Increased concentrations of L-DOPA up to 11 mM L-DOPA/M aldehyde similarly curtailed swelling and mitigated property loss with hydration, but sacrificed initial functional adhesion strength, material modulus and biocompatibility. Taken together, these data support tailored L-DOPA conjugation as a promising approach to enhance the clinical performance of PEG:dextran sealants.

Keywords

Aldehyde; Biocompatibility; Hydrogel; L-3,4-dihydroxyphenylalanine (L-DOPA); Tissue adhesive

1. Introduction

The bioadhesive properties of soft tissue sealants provide a range of potential therapeutic benefits [1-3]. Adhesive interactions between sealants and soft tissues are generally predicated

*Corresponding author Tarek Shazly, 77 Massachusetts Avenue, Building E25, Room 442, Cambridge, MA 02139, Phone: 617-258-8895, Fax: 617-253-2514, shazly@mit.edu.

on an in-situ material transformation, such as the hydroxide-catalyzed ionic polymerization of cyanoacrylate derivatives or the calcium-mediated network assembly of fibrin glues [3,4]. Multiple determinants of sealant performance depend on material reactive chemistry and as a result are challenging to optimize independently, including adhesion strength to target tissue, degradation kinetics and the local biological response [2,5,6]. A family of two-component hydrogels composed of amine-functionalized star polyethylene glycol and dextran aldehyde polymers (PEG:dextran) provides an aldehyde-mediated material system with tunable adhesive and cohesive properties [7-11]. PEG:dextran hydrogels are cohesively crosslinked by imine bonds between amine and aldehyde groups mounted on high molecular weight constituent polymers. An analogous chemistry controls the primary PEG:dextran adhesive mechanism wherein free hydrogel aldehydes bind to tissue amines present on cells or extracellular matrix. Rational adjustment of relative reactive group concentrations of constituent polymers facilitates semi-independent regulation of adhesive and bulk material properties in the PEG:dextran system, and can even do so on an application-specific basis governed by the aldehyde-affinity of targeted soft tissues [7,10,11].

The characteristically high water content of swollen hydrogels traditionally imparts excellent biocompatibility and has made them appealing candidates for biomaterial implants [12-14]. Hydrogels are an attractive material class for sealant applications in particular, as their mechanical properties after swelling are comparable to native soft tissue [15]. Sustained adhesion under physiologic loading implies that a severe mismatch in tissue-material compliances will generate local stress concentrations at the adhesive interface and could cause destruction of underlying tissue architecture and material failure [7,16]. In addition to having bulk mechanical properties in the range of soft tissues, PEG:dextran hydrogels exhibit adjustable, viscoelastic adhesive interactions that confer failure resistance and retention of tissue morphology in ex-vivo tissue-material constructs [7].

While hydrogel swelling is potentially beneficial to both sealant mechanics and biocompatibility, bulk expansion will modulate multiple material properties and may reduce sealant functionality. Here we observe that the adhesive interface between PEG:dextran and duodenal tissue is physically altered and functionally compromised as a result of material swelling. We adopt a biomimetic design strategy to mitigate swelling-induced functional loss, specifically the conjugation of L-3,4-dihydroxyphenylalanine (L-DOPA) within the PEG:dextran network. L-DOPA has been recognized as a key amino acid governing the remarkable wet adhesion capabilities exhibited by marine animals, and has been successfully used as a reactive element in other material systems under hydrated conditions [17-20]. As both cohesion and adhesion of PEG:dextran are mediated by aldehyde-amine interactions, the side groups of L-DOPA make it an ideal network modulator with potential to affect multiple determinants of sealant performance. In this study, the effects of up to 11 mM L-DOPA/M aldehyde on PEG:dextran cohesive and functional adhesive properties under hydrated conditions, as well as biocompatibility, are evaluated and related to surgical sealant potential.

2. Materials and Methods

2.1 Material synthesis

The syntheses of star PEG amine and linear dextran aldehyde polymers along with their copolymerization have been previously described [8,9]. Briefly, eight-arm, 10 kDa star PEG polymer with amine end groups was dissolved in purified water to form a 25 wt. % aqueous solution with a pH of 8.5. Linear dextran (10 kDa) was oxidized with sodium periodate for 5 hours to produce dextran aldehyde polymer (50% oxidation of glucose rings, two aldehyde groups per oxidized glucose ring). The dextran aldehyde polymer was dialyzed for 4 days, lyophilized and reconstituted to form an 8.8 wt. % aqueous solution with a pH of 3.5.

Polymeric constituents spontaneously react to form a two-component hydrogel (PEG:dextran) following a volumetrically-balanced injection from a dual-chamber syringe equipped with a 12-step mixing tip.

A fluorescein-labeled star PEG amine (FITC-PEG) polymer was synthesized to enable fluorescent imaging of PEG:dextran. Star PEG amine (2.4 g) was dissolved in dichloromethane (6 mL), followed by the addition of 15 mg of 6-(fluorescein-5-carboxyamido) hexanoic acid, succinimidyl ester (Invitrogen) and 12 μL triethylamine (Sigma). The solution was stirred continuously at room temperature for 48 hours. The resulting solid after solvent evaporation was dissolved in 100 mL water, dialyzed against 4 L of water (MWCO 500 membranes, Spectrum Labs) and lyophilized for 48 hours (-46°C, 3×10^{-3} mbar). FITC-PEG solutions of 25 wt. % solid content, 0.5% of which were fluorescently labeled, were used for copolymerization with dextran aldehyde solutions.

A series of modified polymers was created by dissolving L-DOPA (Sigma) and lyophilized dextran aldehyde in purified water for 3 hours at 60°C. After full dissolution and mixing, homogeneous solutions were dialyzed for 24 hours against 4 L of water (as above). Solutions were snap frozen in liquid nitrogen and lyophilized (as above). The solid was recovered and reconstituted in water to yield L-DOPA-dextran aldehyde polymer solutions with pH of 3.5. Both L-DOPA stock and L-DOPA-dextran aldehyde were stored under argon until experimental use to prevent oxidation.

2.2 Material characterization: L-DOPA conjugation to dextran aldehyde

Hydrogen NMR was used to characterize L-DOPA conjugation to dextran aldehyde. A series of homogeneous L-DOPA and dextran aldehyde solutions were prepared in D_2O as described above (without solution dialysis) with initial free L-DOPA concentrations of up to 12 wt. %. Pure L-DOPA and dextran aldehyde solutions were also prepared for comparative analyses. Selected solutions of L-DOPA and dextran aldehyde were analyzed immediately following synthesis and after one week storage to verify conjugate stability. NMR spectra were recorded (Bruker Avance 400 MHz instrument) and chemical shifts were reported in ppm relative to the deuterated solvent.

2.3 Functional mechanical testing: ex-vivo burst pressure

Adult Sprague-Dawley rats (250 – 300 g, Charles River Laboratories, MA) were sacrificed by carbon dioxide asphyxiation. The duodenum was excised and immersed in 10 ml Krebs-Henseleit buffer at room temperature. Longitudinal duodenal segments were cut and inserted into a mechanical testing apparatus capable of imparting controlled luminal flow (Bose® Biodynamic Test Instrument, MN). A full-thickness wound was introduced by puncturing of the intestinal wall with an 18 gauge needle. Wounds were then repaired with 200 μl application of sealant to the serosal surface. A five minute sealant curing time was allowed, after which intestinal samples were submerged in phosphate buffered saline (PBS) for up to one hour. The burst pressure of repaired intestinal wounds was measured after predetermined swelling times through gradual increase of lumen pressure developed through restriction of flow (50 ml/min) distal to the sample lumen. Failure of the wound repair site resulted in an immediate loss of luminal pressure and visible PBS leakage at the tissue-material interface. The maximum luminal pressure prior to interface failure indicates the wound burst pressure [7]. All experiments involving animals were approved by the university IACUC protocol and compliant with NIH guidelines for animal care.

2.4 Bulk material properties: swelling ratio and compressive modulus

The dynamic swelling ratio and bulk compressive modulus of modified PEG:dextran hydrogels were examined as a function of swelling time in PBS. Pilot studies were

conducted comparing PEG:dextran swelling in PBS versus aqueous albumin solutions of varying concentration. No significant difference in material swelling behavior was observed over 24 hours in solutions with albumin concentrations ranging from 0 to 5 wt. % (data not shown). As the introduction of proteins into our assays could potentially confound experimental results through tissue-protein interactions, all swelling experiments are performed in PBS.

To measure both PEG:dextran swelling ratio and compressive modulus, cylindrical samples (8 mm diameter, 4 mm height) were prepared with a silicon mold and analyzed after 0, 15, 30, or 60 minutes submersion in 50 mL PBS at room temperature. The dynamic swelling ratio, $q_d(t)$, represents the percent increase in hydrogel weight as a function of swelling time, t, and was calculated from the initial hydrogel weight, $w(0)$, and the post-swelling weight, $w(t)$, as below:

$$q_d(t) = \frac{w(t) - w(0)}{w(0)} \times 100$$

The compressive elastic modulus (E_c) of swollen materials was measured using a mechanical testing system featuring a low force load frame and a hydration chamber (Bose® Biodynamic Test Instrument, MN). The use of a compressive as opposed to tensile testing mode minimized experimental errors that are particularly problematic for swollen hydrogels in hydrated environments, including grip-sample slippage or evolution of stress concentration at the grip-sample interface. Cylindrical material samples were hydrated for various times in 50 mL PBS and then subjected to a ramped compressive displacement (displacement rate of 0.01 mm/sec, maximum displacement of 0.5 mm) while maintained in PBS at room temperature. Sample load and displacement were continuously recorded at a data acquisition rate of 100 points/sec. Acquired mechanical data were transformed to obtain true stress versus strain curves based on swollen sample dimensions. For all materials, stress-strain responses were linear under the described testing conditions and facilitated calculation of E_c via linear regression of the stress-strain response.

2.5 Interfacial material density

An indirect metric of PEG:dextran network density forming the adhesive interface between excised rat duodenal tissue and the material bulk was assessed throughout sample hydration treatments in PBS of up to one hour. Material formulations (200 μl) featuring FITC-PEG amine were applied to the serosal surface and allowed to polymerize for five minutes prior to sample hydration. Following submersion in 50 mL PBS at room temperature for designated swelling times, samples were snap frozen in liquid nitrogen, cryosectioned (20 μm thick sections) and mounted with DAPI-containing mounting medium (Vector Labs). Fluorescent microscopy (Leica) and image analyses software (MetaMorph) were used to depict the interfacial region between PEG:dextran and duodenal tissue. The linescan software feature was used to quantify the fluorescent signal from FITC-PEG amine in the interfacial regime, which was defined as the first 500 μm of material extending normally from the serosal surface. The average fluorescent signal was calculated from 3-5 linescans per image to reflect the PEG:dextran density comprising the adhesive interface.

2.6 Biocompatibility: in-vivo tissue response

The biocompatibility of PEG:dextran adhesives were evaluated by the local tissue response to subcutaneous implants in mice. Briefly, a pocket was created in the dorsal subcutaneous space of anesthetized C57BL/6 mice and 200 μl of material was injected into the pocket using a syringe with a sterilized mixing tip. After nine days the skin and subcutaneous

tissues at the implantation site were harvested. Tissue samples were frozen in liquid nitrogen and stored at -80°C until histological analyses.

Harvested tissues were cryosectioned into 20 μm sections and stained with hematoxylin and eosin using standard methods. Light microscopy was used to assess the local fibrotic response in three randomly selected locations on each tissue section and quantified by the total fibrotic layer thickness (Adobe Photoshop). Zymography was performed using quenched fluorescein-labeled gelatin and fluorescence intensity was quantified and normalized to indicate relative enzymatic activity local to each implanted material (MetaMorph) [21]. Immunohistochemical staining for macrophages was performed as previously described [22]. Briefly, sections were blocked in 10% goat serum for 40 minutes and incubated overnight with a primary antibody for Mac-3 (Biolegend). The samples were then washed three times with PBS and incubated with an anti-rat antibody labeled with alexafluor-594 dye (Invitrogen). After two hours of incubation, the samples were washed extensively and coverslipped in DAPI-containing mounting media (Vector Labs). The fluorescent intensity from alexafluor-594 dye was quantified and normalized to provide a metric of macrophage density at the implantation site.

2.7 Statistical analyses

Analysis of variance (ANOVA) with post-hoc analysis was used to compare sample means, with a resultant $p < 0.05$ taken as statistically significant. Linear regressions between data sets were also performed, for which Pearson's correlation coefficient (R) and associated p-value of the regression have been reported. Here again, $p < 0.05$ is considered statistically significant.

3. Results

3.1 Material characterization

Hydrogen NMR was used to capture the signature spectra of dextran aldehyde (Fig. 1A), L-DOPA (Fig. 1B) and a series of L-DOPA-dextran aldehyde conjugates. A diagnostic signal for the imine proton present in the conjugate form (8.3 ppm) was integrated against the three aromatic protons of L-DOPA (6.6 to 6.9 ppm) to determine the extent and stability of conjugation [23]. In a system exhibiting complete L-DOPA conjugation, a ratio of 3:1 between the integrals of the aromatic L-DOPA and imine bond peaks would be expected and was found (Fig. 1C), with conjugation stability verified following one week of solution storage. Conversely, when conjugation is not complete and L-DOPA exists in both free and conjugated forms, the integrals of the imine and aromatic peaks reflect the relative amount of conjugation in the material system. Other chemical interactions within our material system are possible, including hemiacetal linkages and L-DOPA self polymerization, and may contribute to L-DOPA incorporation within PEG:dextran. Imine bond formation was selected as the diagnostic signal for material characterization due to the emergence of the expected and nearly exact 3:1 integral ratio at low L-DOPA concentrations (< 1 wt. % L-DOPA) and the continuity this metric observed throughout the employed concentration range.

The reaction efficiency nonlinearly decreased with initial L-DOPA concentration ranging from 0.1 to 12 wt. %, with only 10.3 % conjugation achieved in the most concentrated solution (Fig. 1D). Four L-DOPA-dextran aldehyde conjugates with initial L-DOPA concentrations ranging from 0 to 6 wt. % were synthesized for further study. The molar ratios of L-DOPA to aldehyde groups span 0 to 11 mM L-DOPA/M aldehyde and are used to denote material composition in the remainder of this work (Table 1).

3.2 Effect of hydration on adhesive closure of intestinal puncture wounds

The ex-vivo burst pressure of repaired puncture wounds following interfacial hydration signifies the potential of adhesive sealants to mitigate tissue dehiscence or leakage in multiple clinical scenarios. Intestinal samples were wounded, repaired with PEG:dextran sealants and fully submerged in PBS for up to one hour prior to failure testing. The failure resistance of wounds repaired with unmodified PEG:dextran monotonically decreased with swelling time and exhibited a $39 \pm 18\%$ reduction in burst pressure following one hour (Fig. 2A). The effect of swelling time on L-DOPA-PEG:dextran was markedly different than the neat hydrogel, as the burst pressure of the 3 mM conjugate only varied between 66 ± 6.7 and 77 ± 9.7 mmHg with no discernable trend over the observation time. Higher L-DOPA concentrations also stabilized wound burst pressure throughout hydration, although the diminished initial performance of 8 and 11 mM conjugates compared to unmodified PEG:dextran indicates a loss of functional sealant potential with excessive doping.

3.3 Material response to hydration: dynamic swelling and compressive modulus

The dynamic swelling ratio (q_d) and compressive modulus (E_c) of PEG:dextran sealants were monitored throughout material sample hydration in PBS. Unmodified PEG:dextran exhibited the greatest swelling, with a q_d of $34.9 \pm 1.5\%$ after one hour of hydration, while conjugate q_d was approximately half that value for all tested L-DOPA concentrations (Fig. 2B). After 24 hours, the q_d for unmodified PEG:dextran was $53.2 \pm 4.9\%$, while conjugate q_d was comparatively lower and ranged from $27.4 \pm 3.5\%$ to $32.9 \pm 3.8\%$ (data not shown). All materials exhibited a reduction in E_c after one hour swelling time (Fig. 2C), with a significantly greater loss of stiffness in the unmodified PEG:dextran ($86.2 \pm 4.1\%$ reduction in E_c) as compared to L-DOPA conjugates (maximum E_c reduction of $44.8 \pm 3.2\%$ in the 11 mM conjugate). As with swelling, initial trends in modulus were retained over 24 hours, where unmodified PEG:dextran exhibited an E_c of 28.3 ± 3.7 kPa and the conjugate family had significantly higher E_c that ranged from 94 ± 8.6 kPa to 103 ± 10.9 kPa (data not shown). Although material variants exhibited similar E_c at early swelling times (15 – 30 minutes), the loss of E_c relative to the pre-swelling value was always greatest for the unmodified PEG:dextran; this trend reflects the differential effect of swelling. L-DOPA conjugation appreciably curtailed both material swelling and concurrent decrease in elastic modulus over the one hour hydration treatment, with minimal variation of either phenomenon in the examined concentration range of 3 to 11 mM L-DOPA/M aldehyde.

3.4 Effect of L-DOPA on interfacial material density

Material density at adhesive interfaces between PEG:dextran variants and excised duodenal tissue was assessed as a function of swelling time. The differential interfacial hydration responses of unmodified PEG:dextran and the 3 mM conjugate are visually evident (Fig. 3A), with quantification of interfacial regime fluorescence suggesting both a swelling-induced loss of PEG:dextran network density and the significant mitigation of this loss with L-DOPA incorporation (Fig. 3B). A negative correlation between measured interfacial density and material q_d throughout hydration was expected and verified, as the reduction in bulk density with increased swelling is reflected in the material morphology forming the adhesive interface (Fig. 3C). Following one hour swelling treatments, interfacial material density correlates well with the burst pressure of repaired wounds across the L-DOPA-PEG:dextran variants, highlighting the influence of interfacial material properties on sealant performance (Fig. 3D).

3.5 Pre- and post-swelling correlates to burst pressure

The pre-swelling burst pressures of duodenal wounds repaired with modified PEG:dextran monotonically decreased with L-DOPA content, as the most concentrated conjugate failed at

a lumen pressure of 47.1 ± 6.6 mmHg compared to 81.4 ± 5.6 mmHg for the unmodified material (Fig. 2A, 0 min swelling time). Correlation of pre-swelling burst pressure and E_c extended across the material series, and may reflect the common dependence of adhesive and cohesive bond formation on aldehyde-amine crosslinking – both events are compromised with L-DOPA conjugation to the dextran aldehyde constituent prior to network formation (Fig. 4A). While the pre-swelling performance of PEG:dextran variants can be understood in these terms, no direct relationship between burst pressure and E_c persisted throughout material swelling. However, the total change of burst pressure after one-hour hydration correlated strongly with the total extent of material swelling (Fig. 4B) and the concomitant reduction of E_c (Fig. 4C). These correlations suggest that initial sealant potential is diminished by swelling, and that L-DOPA simultaneously curtails swelling and abrogates functional loss in PEG:dextran.

3.6 Effect of L-DOPA on material biocompatibility

The efficacy of strongly adherent surgical sealants is often limited by the associated tissue response. PEG:dextran sealant biocompatibility was examined through subcutaneous material implantations in mice. Three indicators of local tissue inflammation were assessed based on microscopic analyses of stained sections, including the fibrotic layer thickness, enzymatic activity and macrophage presence. PEG:dextran implants elicited a fibrotic response to an extent dependent on L-DOPA content (Fig. 5A). The fibrous layer thickness incited by unmodified PEG:dextran implantations was minimal (90 ± 40 µm), while 3 and 8 mM conjugates caused slightly increased thicknesses of 280 ± 40 µm and 190 ± 60 µm, respectively. The tissue response to 11 mM implants was an order of magnitude more severe than to unmodified PEG:dextran (fibrotic thickness of 890 ± 70 µm), suggesting that hydrogel biocompatibility is compromised by excessive L-DOPA conjugation (Fig. 5B).

Excessive inflammatory cell-mediated proteolysis impedes wound repair via matrix metalloprotease (MMP) cleavage of extracellular matrix proteins. MMP activity is often elevated during surgery and particularly problematic at surgical anastomoses because of the potential to destabilize wound sites and facilitate tissue dehiscence [24,25]. The gelatinase activity in local tissues following PEG:dextran implantations were measured using in-situ zymography (Fig. 6A). The fluorescent intensity indicative of gelatinase activity monotonically rose with L-DOPA content, suggesting an increased stimulation of pro-inflammatory mediators and polymorphonuclear leukocytes (Fig. 6B).

Macrophages migrate to implantation sites and serve numerous functions associated with tissue inflammation, including the regulation of fibroblast activity, secretion of MMPs and phagocytosis of material debris [26,27]. Fluorescent mac-3 labeling demonstrated that macrophages were present at various densities following the implantation of PEG:dextran materials (Fig. 7A). The density of macrophages in local tissues was low and statistically indistinguishable until the highest L-DOPA concentration was used (Fig. 7B). Macrophage density was approximately six-fold greater in tissues subjected to 11 mM L-DOPA/M aldehyde implantations compared to unmodified PEG:dextran, which again suggests that excessive L-DOPA content will substantially reduce material biocompatibility.

4. Discussion

Soft tissue sealant efficacy depends on the local environment following implantation, with a range of tissue chemistries, surface morphologies, pH and mechanical forces encountered in routine use [6]. Common among all biological sealant applications is the eventual exposure of material to physiological fluids. We posited that the adhesive interactions between soft tissues and hydrogel-based sealants would be altered significantly by material swelling in a manner that limits efficacy. In the present study, the reduction of PEG:dextran density at the

adhesive interface is measured throughout initial material swelling and correlated to the concomitant loss of sealant function ex-vivo. Although hydrogels are a biocompatible material class for sealant development, these data suggest that their high characteristic swelling may limit sealant function, motivating the pursuit for techniques of post-swelling hydrogel property enhancement.

Nature often inspires engineering solutions to dilemmas of biomaterial design. In this work we adopted a biomimetic approach to bulk PEG:dextran modification that was previously used in other material systems. Multiple variants of the adhesive foot protein 3 in *Mytilus californianus* (Mcfp-3) have been implicated in marine mussel adhesion, with all proteins containing L-DOPA-rich domains [28]. Reports on both surface- and bulk-incorporated L-DOPA have collectively demonstrated modulated interactions with both organic and inorganic surfaces and within material networks [19,29-31]. Prior studies have found that L-DOPA films can be applied to materials through simple dip-coating and promote adherence to surfaces of metals, ceramics, polymers and various cell lines [31]. The presently examined L-DOPA conjugation to dextran aldehyde further recapitulates mussel adhesive plaques in which adhesive proteins are embedded within polysaccharide matrices to facilitate flexibility and failure resistance at the point of contact with underlying substrates [32].

The addition of L-DOPA to the PEG:dextran system affects material cohesive and adhesive properties in a complex manner. Network cohesion, as reflected by pre-swelling E_c, falls in a concentration-dependent manner that suggests L-DOPA reduces crosslinking by competing with polymer amines for network-forming aldehydes. The increased size of the side group raises the potential for steric inhibition of crosslinking, further affecting cohesion. In an analogous manner pre-swelling burst pressure falls with L-DOPA conjugation, as PEG:dextran aldehyde-mediated adhesion to soft tissue is observably compromised with the reduction in material free aldehyde density [7,11].

Interestingly, pre-swelling correlation between E_c and burst pressure of repaired wounds was observed, despite the different nature of these properties. This correlation is again reflective of aldehyde group mediation of both the internal material crosslinking (with constitutive PEG amine groups) and the external adhesive tissue crosslinking (with tissue-present amine groups). However, correlation did not persist throughout the swelling period of observation. With time, all material variants exhibited greater percent decrease in E_c as compared to the measured decrease in burst pressure. We posit that differential trends throughout swelling arise because distinct phenomena mediate bulk and adhesive properties. Compressive testing of elastic moduli only probes the response of the bulk material, while burst pressure reflects a combination of bulk and adhesive interfacial responses and ultimately resistance to interfacial failure. These data suggest that burst pressure, which is heavily influenced by tissue-material interfacial bond density, varies significantly with material chemistry but is comparatively insensitive to swelling time. Conversely, E_c is governed primarily by entropic as opposed to energetic resistance at low strains in hydrogels, and thus varies markedly with swelling presumably due to concomitant network chain reconfiguration [33].

Despite the apparent interference with aldehyde-mediated crosslinking, our study found that 3 mM L-DOPA/M aldehyde within PEG:dextran was minimally disruptive to initial sealant potential and promoted retention of material stiffness, interfacial morphology and burst pressure throughout hydration, ultimately conferring enhanced post-swelling function. PEG:dextran properties, specifically those relevant to sealant applications, are presumably stabilized by both the reduction in material swelling and L-DOPA-mediated bonding, which could include internal interactions with self and external interactions with the tissue surface [34,35].

We chose to characterize the biocompatibility of PEG:dextran conjugates in an animal model that is not reflective of a specific clinical scenario. Given the multitude of potential applications of surgical sealants, a general assay of biocompatibility such as represented by a subcutaneous implantation model should precede more specific animal models. Moreover, the subcutaneous model allows one to divorce the functional efficacy of a particular material formulation from the base biocompatibility, while more complex models would instead reflect a combination of sealant performance, biocompatibility and functional effects in a specific clinical application.

Macrophage localization represents a metric of particular interest due to the pivotal role these cells play in the tissue response to implanted materials, including inflammatory mediation and formation of a fibrous capsule. Macrophages complex with fibronectin through cell surface integrin receptors, leading to various intracellular signaling events and the eventual upregulation of inflammatory cytokines [36]. Macrophages are crucial mediators in the immune response, as they ensure phagocytosis of foreign debris, release biologically active compounds and present antigens to immunecompetent cells. Thus, macrophage activation may influence nearly every aspect of both normal and abnormal immune and inflammatory responsiveness, and is of paramount importance in assessing general biocompatibility. [37]

Although 3 mM L-DOPA/M aldehyde had only a minor effect of tissue response, multiple tissue response metrics indicated that PEG:dextran biocompatibility was significantly reduced following implantation of 11 mM L-DOPA/M aldehyde conjugate. The reduction in biocompatibility at high doping levels can be readily attributed to two potential sources: L-DOPA itself or the aldehyde groups liberated by the aforementioned disruption of PEG:dextran network formation. The latter of these possibilities is supported by previous work, which showed a reduction in PEG:dextran biocompatibility with increasing free aldehyde content [10]. Irrespective of the underlying cause, trends in both the local tissue response and burst pressure data provide incentive to carefully adjust L-DOPA concentration within PEG:dextran as a means to enhance post-swelling sealant performance.

A limitation of this work is the swelling times over which material behavior was assessed. We were only able to analyze sealant function for one hour after swelling given the need to preserve tissue integrity. At these short times, the hydrogels do not reach equilibrium swelling states. Moreover, other dynamic processes, which occur over longer times, such as hydrolytic bond degradation and wound healing, are not considered here, yet will undoubtedly influence interfacial failure resistance. Long term sealant behavior can however be extrapolated from the presented data set, as we would predict that materials which ultimately swell less would better maintain their maximal functional potential.

Biomaterials must be evaluated at physiologically-relevant states to understand their true clinical potential. Hydrogels are appealing platforms for development of implants that interact intimately with soft tissues because of their composition and associated biocompatibility; yet high material swelling can strongly influence adhesive interactions. The present study demonstrates that low concentrations of L-DOPA within PEG:dextran can effectively combat functional loss related to swelling. Moreover, when viewed in concert with previous studies on PEG:dextran, this work adds to the collection of general strategies for improving sealant functionality, namely maintaining tissue viscoelasticity after adhesion, considering tissue-specific biochemistry for targeted adhesion and now limiting material swelling in-situ [7,10]. The results of this work provide a general impetus to regulate material swelling in order to promote the retention of functional tissue-material adhesive interactions, and as such may be relevant to other hydrogel-based adhesive systems.

5. Conclusion

It is recognized that the local physiological environment can modulate biomaterial implants in a variety of ways and often to an extent which diminishes their therapeutic potential. In-situ swelling of a hydrogel-based soft tissue sealant represents a biologically-induced dynamic which may reduce therapeutic potential in applications involving substantial physiological loads. We demonstrate that PEG:dextran sealants undergo a swelling-induced reduction of material density at the adhesive interface and suffer a correlated loss of function in an ex-vivo model. Conjugation of L-DOPA to PEG:dextran limits material swelling and enhances hydrated sealant performance. Functionally effective doping levels of 3 mM L-DOPA/M aldehyde within PEG:dextran did not substantially alter biocompatibility as indicated by the subcutaneous tissue response to material implants. In general, L-DOPA-based modification provides a means to safely enhance post-swelling adhesive properties and as such is a promising approach to advance surgical sealant design.

Acknowledgments

References

1. Buchta C, Hedrich HC, Macher M, Hocker P, Redl H. Biochemical characterization of autologous fibrin sealants produced by CryoSeal and Vivostat in comparison to the homologous fibrin sealant product Tissucol/Tisseel. Biomaterials. 2005; 26(31):6233–41. [PubMed: 15921738]

2. Jackson MR. Tissue sealants: current status, future potential. Nat Med. 1996; 2(6):637–8. [PubMed: 8640550]

3. Silver FH, Wang MC, Pins GD. Preparation and use of fibrin glue in surgery. Biomaterials. 1995; 16(12):891–903. [PubMed: 8562777]

4. Samuel NT, Vailhe E, Vailhe C, Vetrecin R, Liu C, Maziarz PE. Comprehensive characterization of the effect of tissue storage conditions on tissue-adhesive interaction. J Biomater Sci Polym Ed. 2008; 19(11):1455–68. [PubMed: 18973723]

5. Ciapetti G, Stea S, Cenni E, Sudanese A, Marraro D, Toni A, Pizzoferrato A. Cytotoxicity testing of cyanoacrylates using direct contact assay on cell cultures. Biomaterials. 1994; 15(1):63–7. [PubMed: 8161661]

6. Sierra, D.; S, R. Surgical Adhesives and Sealants. Lancaster: Technomic Publishing AG; 1996.

7. Shazly TM, Artzi N, Boehning F, Edelman ER. Viscoelastic adhesive mechanics of aldehyde-mediated soft tissue sealants. Biomaterials. 2008; 29(35):4584–91. [PubMed: 18804861]

8. Bhatia SK, Arthur SD, Chenault HK, Figuly GD, Kodokian GK. Polysaccharide-based tissue adhesives for sealing corneal incisions. Curr Eye Res. 2007; 32(12):1045–50. [PubMed: 18085468]

9. Bhatia SK, Arthur SD, Chenault HK, Kodokian GK. Interactions of polysaccharide-based tissue adhesives with clinically relevant fibroblast and macrophage cell lines. Biotechnol Lett. 2007; 29(11):1645–9. [PubMed: 17636385]

10. Artzi N, Shazly T, Baker A, Bon A, Edelman ER. Aldehyde-Amine Chemistry Enables Modulated Biosealants with Tissue-Specific Adhesion. Advanced Materials. 2009; 21(32-33):3399–3403. [PubMed: 20882504]

11. Artzi N, S T, Crespo C, Chenault HK, Edelman ER. Characterization of Star Adhesive Sealant Based On PEG:Dextran Hydrogels. Macromol Biosci. 2009 in press.

12. Peppas NA, Sahlin JJ. Hydrogels as mucoadhesive and bioadhesive materials: a review. Biomaterials. 1996; 17(16):1553–61. [PubMed: 8842358]

13. Suggs LJ, Shive MS, Garcia CA, Anderson JM, Mikos AG. In vitro cytotoxicity and in vivo biocompatibility of poly(propylene fumarate-co-ethylene glycol) hydrogels. J Biomed Mater Res. 1999; 46(1):22–32. [PubMed: 10357132]

14. Liu Y, Chan-Park MB. Hydrogel based on interpenetrating polymer networks of dextran and gelatin for vascular tissue engineering. Biomaterials. 2009; 30(2):196–207. [PubMed: 18922573]

15. Bader RA. Synthesis and viscoelastic characterization of novel hydrogels generated via photopolymerization of 1,2-epoxy-5-hexene modified poly(vinyl alcohol) for use in tissue replacement. Acta Biomater. 2008

16. Hilborn J, Bjursten LM. A new and evolving paradigm for biocompatibility. J Tissue Eng Regen Med. 2007; 1(2):110–9. [PubMed: 18038399]

17. Burke SA, Ritter-Jones M, Lee BP, Messersmith PB. Thermal gelation and tissue adhesion of biomimetic hydrogels. Biomed Mater. 2007; 2(4):203–10. [PubMed: 18458476]

18. Hwang DS, Sim SB, Cha HJ. Cell adhesion biomaterial based on mussel adhesive protein fused with RGD peptide. Biomaterials. 2007; 28(28):4039–46. [PubMed: 17574667]

19. Lee BP, Dalsin JL, Messersmith PB. Synthesis and gelation of DOPA-modified poly(ethylene glycol) hydrogels. Biomacromolecules. 2002; 3(5):1038–47. [PubMed: 12217051]

20. Waite JH. Reverse engineering of bioadhesion in marine mussels. Ann N Y Acad Sci. 1999; 875:301–9. [PubMed: 10415577]

21. Gawlak M, Gorkiewicz T, Gorlewicz A, Konopacki FA, Kaczmarek L, Wilczynski GM. High resolution in situ zymography reveals matrix metalloproteinase activity at glutamatergic synapses. Neuroscience. 2009; 158(1):167–76. [PubMed: 18588950]

22. Baker AB, Groothuis A, Jonas M, Ettenson DS, Shazly T, Zcharia E, Vlodavsky I, Seifert P, Edelman ER. Heparanase alters arterial structure, mechanics, and repair following endovascular stenting in mice. Circ Res. 2009; 104(3):380–7. [PubMed: 19096032]

23. Pretsch, E.; B, P.; Affolter, C. Structure determination of organic compounds. Berlin: Springer-Verlag; 2000.

24. Pasternak B, Rehn M, Andersen L, Agren MS, Heegaard AM, Tengvall P, Aspenberg P. Doxycycline-coated sutures improve mechanical strength of intestinal anastomoses. Int J Colorectal Dis. 2008; 23(3):271–6. [PubMed: 18043927]

25. Nugent HM, Sjin RT, White D, Milton LG, Manson RJ, Lawson JH, Edelman ER. Adventitial endothelial implants reduce matrix metalloproteinase-2 expression and increase luminal diameter in porcine arteriovenous grafts. J Vasc Surg. 2007; 46(3):548–556. [PubMed: 17826244]

26. Glaros T, Larsen M, Li L. Macrophages and fibroblasts during inflammation, tissue damage and organ injury. Front Biosci. 2009; 14:3988–93. [PubMed: 19273328]

27. Shima I, Katsuda S, Ueda Y, Takahashi N, Sasaki H. Expression of matrix metalloproteinases in wound healing after glaucoma filtration surgery in rabbits. Ophthalmic Res. 2007; 39(6):315–24. [PubMed: 17957131]

28. Lin Q, Gourdon D, Sun C, Holten-Andersen N, Anderson TH, Waite JH, Israelachvili JN. Adhesion mechanisms of the mussel foot proteins mfp-1 and mfp-3. Proc Natl Acad Sci U S A. 2007; 104(10):3782–6. [PubMed: 17360430]

29. Dalsin JL, Hu BH, Lee BP, Messersmith PB. Mussel adhesive protein mimetic polymers for the preparation of nonfouling surfaces. J Am Chem Soc. 2003; 125(14):4253–8. [PubMed: 12670247]

30. Statz AR, Meagher RJ, Barron AE, Messersmith PB. New peptidomimetic polymers for antifouling surfaces. J Am Chem Soc. 2005; 127(22):7972–3. [PubMed: 15926795]

31. Lee H, Dellatore SM, Miller WM, Messersmith PB. Mussel-inspired surface chemistry for multifunctional coatings. Science. 2007; 318(5849):426–30. [PubMed: 17947576]

32. Silverman HG, Roberto FF. Understanding marine mussel adhesion. Mar Biotechnol (NY). 2007; 9(6):661–81. [PubMed: 17990038]

33. Sarvestani AS, He X, Jabbari E. Viscoelastic characterization and modeling of gelation kinetics of injectable in situ cross-linkable poly(lactide-co-ethylene oxide-co-fumarate) hydrogels. Biomacromolecules. 2007; 8(2):406–15. [PubMed: 17253761]

34. Usha R, Rajaram A, Ramasami T. Stability of collagen in the presence of 3,4-dihydroxyphenylalanine (DOPA). J Photochem Photobiol B. 2009; 97(1):34–9. [PubMed: 19716709]

35. Gade JN, Fellman JH, Bentley JP. The stabilization of fibrillar collagen matrices with 3,4-dihydroxyphenylalanine. J Biomed Mater Res. 1991; 25(7):799–811. [PubMed: 1918101]

36. Kenneth, Ward W. A review of the foreign-body response to subcutaneously-implanted devices: the role of macrophages and cytokines in biofouling and fibrosis. J Diabetes Sci Technol. 2008; 2(5):768–77. [PubMed: 19885259]

37. Anderson, J. Biomaterials Science: Inflammation, wound healing, and the foreign-body response. San Diego: Elsevier Academic Press; 2004.
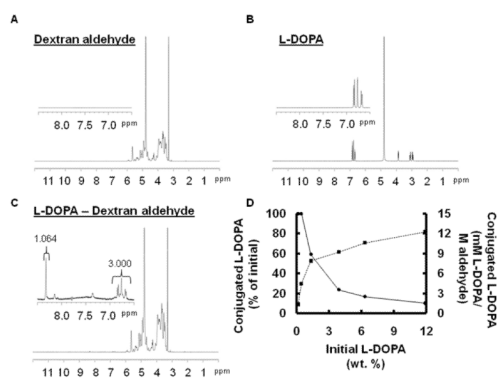
Figure 1.
(A) NMR spectra of dextran aldehyde, (B) L-DOPA, and (C) a 0.3 wt % conjugation of L-DOPA to dextran aldehyde. Following conjugation, the triplet peaks (6.6–6.9 ppm) indicate total L-DOPA content, whereas the imine peak (8.3 ppm) was diagnostic of conjugated L-DOPA. The ratio between the integrals of the triplet and imine peaks was used to calculate the extent of conjugation following reaction, with a 3:1 ratio indicating complete conjugation. (D) The % of initial L-DOPA (▲) and the molar ratio of L-DOPA to constituent aldehyde groups (■) conjugated after reaction are presented as a function of initial L-DOPA concentration to indicate the variation of reaction efficiency and product
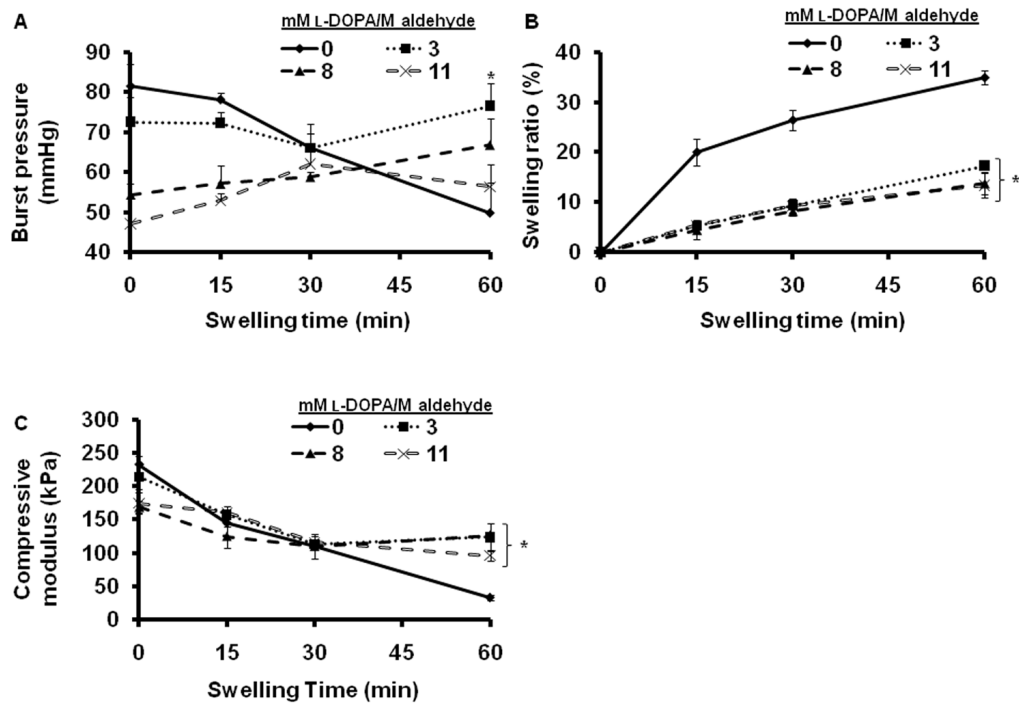
Figure 2.
(A) The *ex vivo* burst pressure of repaired rat duodenal wounds was assessed after various swelling times. Puncture wounds were repaired with PEG:dextran formulations featuring L-DOPA at molar concentrations of 0 (◆), 3 (■), 8 (▲), or 11 (*x*) m*M* L-DOPA/M aldehyde. After sample treatment for the designated swelling time, sample lumens were perfused with PBS (50 mL/min) and gradually pressurized. The pressure at which the wound repair site mechanically failed was recorded as the burst pressure. (B) The dynamic swelling ratio, q_d, and the (C) compressive elastic modulus, E_c, of the same materials were also assessed as function of swelling time. Error bars in all graphs represent 1 standard error of measurement ($n = 3$ to 5). * indicates $p < 0.05$ determined by ANOVA with *post hoc* analysis when compared with 60-min swelling time for unmodified PEG:dextran
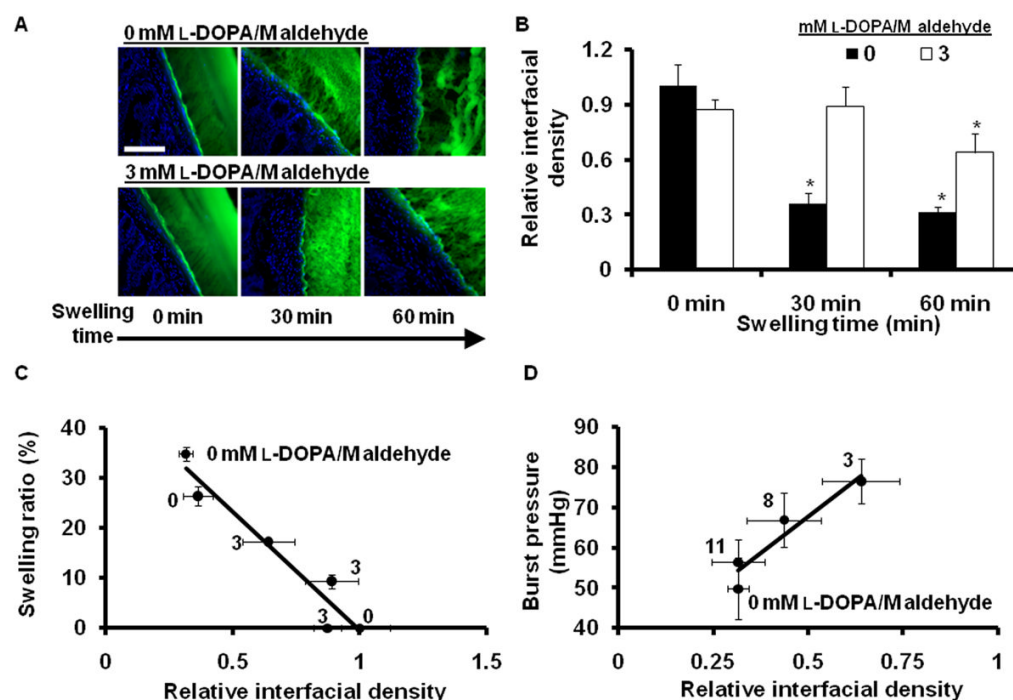
Figure 3.
(A) The density of material forming the adhesive interface between excised duodenal tissue (cell nuclei stained blue with DAPI) and material bulk (FITC-labeled PEG:dextran variants appear green) varied with swelling time. The interfacial material density of unmodified PEG: dextran (upper panels) visibly diminished with swelling time, whereas the interfacial density of the 3 m*M* L-DOPA/M aldehyde variant (bottom panels) remained comparatively stable. Scale bar = 1000 μm and applies to all images. (B) The relative density of material extending normally from the tissue surface (500 μm) was assessed with analytical microscopy and presented at select swelling times for unmodified PEG:dextran and the 3 m*M* L-DOPA/M aldehyde conjugate. Error bars represent 1 standard error of measurement ($n = 4$). * indicates $p < 0.05$ determined by ANOVA with *post hoc* analysis when compared to 0-min swelling time for each material. (C) The dynamic swelling ratio, q_d, inversely correlates ($R = -0.96$, $p < 0.05$, solid line represents linear fit of data) to the interfacial densities in the above images (A), supporting the intuitive loss of material density with swelling at the adhesive interface. (D) Linear correlation ($R = 0.92$, $p < 0.05$, solid line represents linear fit of data) exists between sample burst pressure and interfacial density across all material samples after 1-h hydration. Data point labels (C and D) reflect material conjugation level (m*M* L-DOPA/M aldehyde)
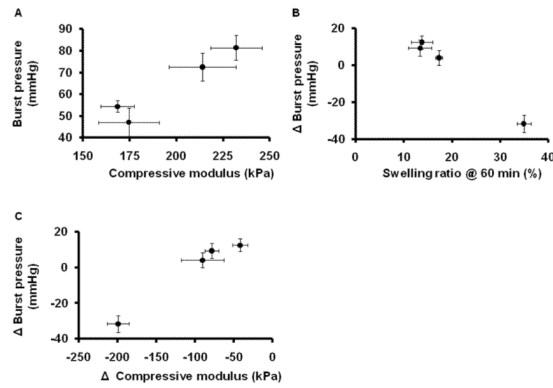
Figure 4.
(A) Before material hydration, positive correlation ($R = 0.96$, $p < 0.05$) exists between the material compressive modulus, E_c, and the wound burst pressure when repaired with the corresponding PEG:dextran formulation. (B) After a full hour of hydration, the extent to which initial burst pressure changed from the preswell value negatively correlated ($R = -0.99$, $p < 0.05$) to material swelling ratio, q_d, and (C) positively correlated ($R = 0.98$, $p < 0.05$) to the change in material modulus. Error bars represent 1 standard error of measurement in all graphs ($n = 3$ to 5)
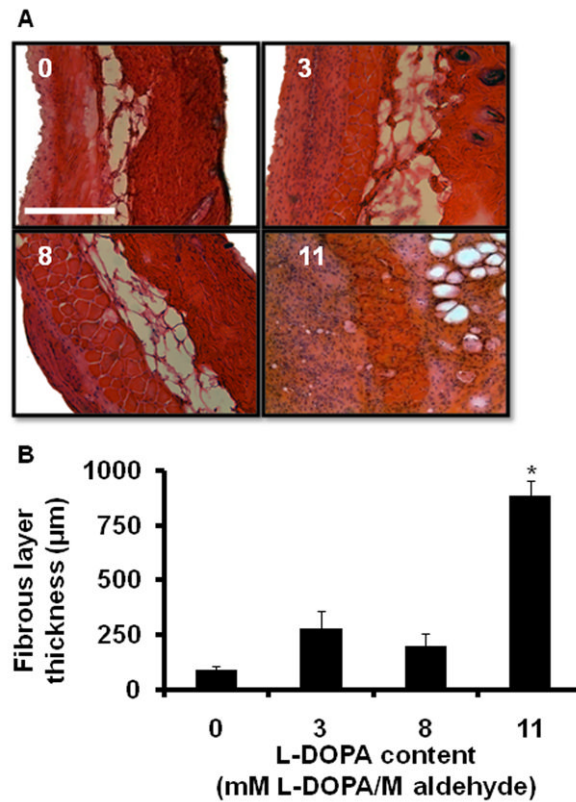
Figure 5.
(A) Tissue fibrous layer thickness local to PEG:dextran variants increases with L-DOPA content. Mice were implanted with material (200 μL) subcutaneously and tissues were harvested after 9 days. Hematoxylin and eosin stained sections of tissue demonstrate increased cellular infiltration and formation of fibrous tissue surrounding the implanted material. Scale bar = 500 μm and applies to all images. (B) Fibrous layer thickness was measured and found to be significantly increased in 11 m*M* L-DOPA/M aldehyde conjugate. Error bars represent 1 standard error of measurement ($n = 4$ to 5). * indicates $p < 0.05$ determined by ANOVA with *post hoc* analysis when compared to unmodified PEG:dextran
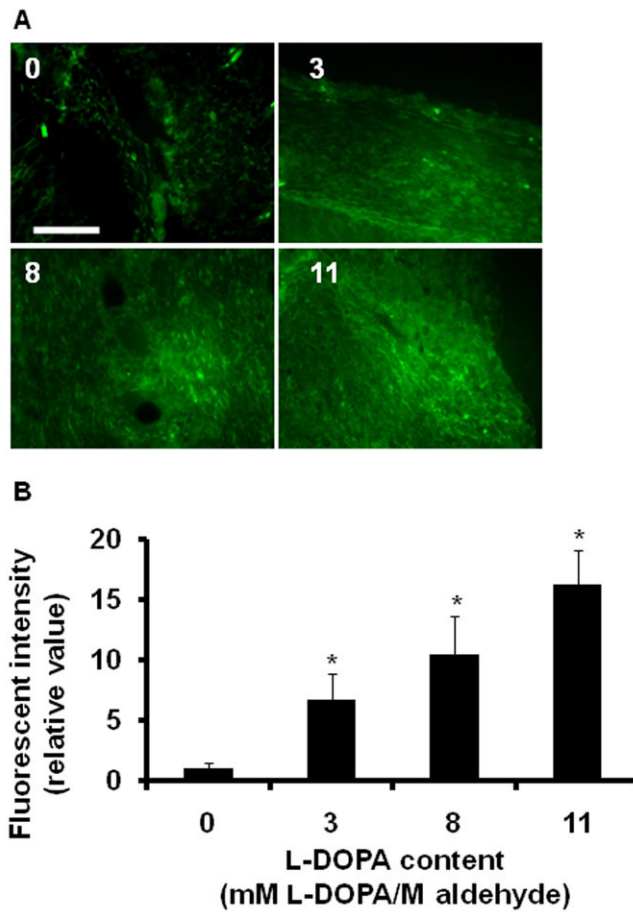
Figure 6.
(A) Analysis of gelatinase activity in subcutaneous tissue following implantation of PEG:dextran variants. *In situ* zymography with an internally quenched FITC-labeled gelatin substrate indicated gelatinase activity. Scale bar = 1000 μm and applies to all images. (B) L-DOPA conjugation within PEG:dextran stimulated local tissue gelatinase activity as indicated by a monotonic rise of relative fluorescent measurements with increasing L-DOPA concentration. Error bars represent 1 standard error of measurement (n = 4 to 5). * indicates $p < 0.05$ determined by ANOVA with *post hoc* analysis when compared with unmodified PEG:dextran
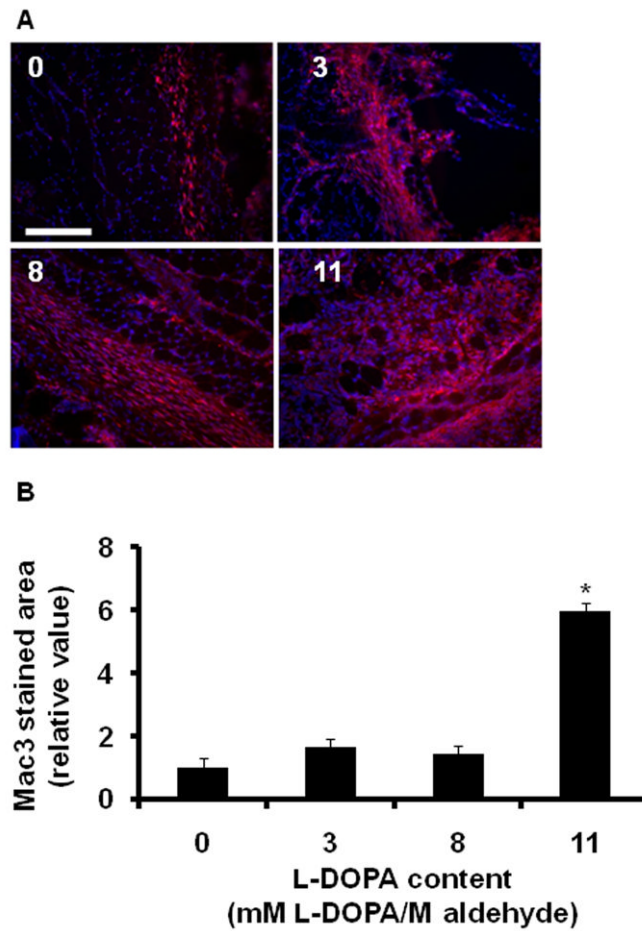
Figure 7.
(A) Macrophage infiltration (red by immunofluorescent staining for Mac-3, cell nuclei stained blue with DAPI) varied among subcutaneous implantations of PEG:dextran materials. Scale bar = 1000 μm and applies to all images. (B) Macrophage infiltration was quantified with analytical microscopy and found to be increased in 11 m*M* L-DOPA/M aldehyde content material. Error bars represent 1 standard error of measurement (*n* = 4 to 5). * indicates *p* < 0.05 determined by ANOVA with *post hoc* analysis when compared with unmodified PEG:dextran.

Table 1

Constituent dextran aldehyde properties (molecular weight, oxidation state, and solid content) were constant across material variants, while initial L-DOPA content ranged from 0 to 60 mM L-DOPA/M aldehyde. The extent of conjugation in the modified dextran aldehyde polymer product was determined by hydrogen NMR and ranged from 0 to 11 mM L-DOPA/M aldehyde.

Dextran aldehyde			L-DOPA conjugation		
Molecular weight (kDa)	Oxidation state (%)	Solid content (wt. %)	Initial molar ratio (mM L-DOPA/M aldehyde)	Final molar ratio (mM L-DOPA/M aldehyde)	Reaction efficiency (%)
10	50	8.8	0	0	-
10	50	8.8	3	3	100
10	50	8.8	20	8	40
10	50	8.8	60	11	18